The Journal of Chemical Physics

RESEARCH ARTICLE | JANUARY 23 2024

The overlooked role of excited anion states in NiO_2^- photodetachment

C. Annie Hart ; Anthony W. Schlimgen ; Diep Bich Dao; Kade Head-Marsden ; Richard Mabbs

J. Chem. Phys. 160, 044304 (2024)
https://doi.org/10.1063/5.0188066

The Journal of Chemical Physics ARTICLE pubs.aip.org/aip/jcp

The overlooked role of excited anion states in NiO_2^- photodetachment

Cite as: J. Chem. Phys. 160, 044304 (2024); doi: 10.1063/5.0188066
Submitted: 18 November 2023 • Accepted: 1 January 2024 •
Published Online: 23 January 2024

C. Annie Hart, Anthony W. Schlimgen, Diep Bich Dao, Kade Head-Marsden, and Richard Mabbs[a]

AFFILIATIONS

Department of Chemistry, Washington University in St. Louis, St. Louis, Missouri 63130-4862, USA

[a]Author to whom correspondence should be addressed: mabbs@wustl.edu

ABSTRACT

Photodetachment spectra of anionic species provide significant insights into the energies and nature of ground and excited states of both the anion and resultant neutral molecules. Direct detachment of the excess electron to the continuum may occur via formally allowed or forbidden transitions (perhaps as the result of intensity borrowing through vibronic coupling). However, alternate indirect pathways are also possible and often overlooked. Here, we report a two-dimensional photoelectron spectral study, combined with correlated electronic structure calculations, to elucidate the nature of photodetachment from NiO_2^-. The spectra are comprised of allowed and forbidden transitions, in excellent agreement with previously reported slow electron velocity mapped imaging spectra of the same system, which were interpreted in terms of direct detachment. In the current work, the contributions of indirect processes are revealed. Measured oscillations in the branching ratios of the spectral channels clearly indicate non-direct detachment processes, and the electronic structure calculations suggest that excited states of the appropriate symmetry and degeneracy lie slightly above the neutral ground state. Taken together, the results suggest that the origin of the observed forbidden transitions is the result of anion excited states mediating the electron detachment process.

INTRODUCTION

Low-lying excited anion states represent energy regimes in which "free" electrons can strongly interact with neutral molecules. These electronic resonances represent potential doorway states for electron capture, are responsible for significant electron-molecule scattering, and have a strong influence in photodetachment. Some recent examples include both molecular anion[1,2] and cluster anion detachment.[3,4] Calculations for such states can be challenging, and benchmarking spectroscopic information on the properties of these resonances is not common. Although time consuming, measurements made over a range of photon energies (as required to produce a 2D-PES) are particularly powerful in revealing the presence and effect of excited anion states or resonances embedded in the continuum.[5] In this work, we report a two-dimensional photoelectron spectroscopic (2D-PES)[6–10] study of the nickel dioxide anion, NiO_2^-. Excitation energy dependent fluctuations in the branching ratios of different detachment channels identify the presence of metastable anion excited states mediating the detachment process. In fact, the 2D-PES provides information on the excited state energies and vibrational frequencies. The nature of the excited anion states, and their proximity to the neutral ground state of NiO_2, is further revealed through multireference configuration interaction (CI) calculations. These calculations also yield details of the anion state potential energy variation along the symmetric stretching and bending coordinates that account for the presence of forbidden transitions in the detachment spectra. Together, this combination of experiment and theory strongly implicates the role of electronic resonances embedded in the continuum as an explanation for the recently reported observation of forbidden bending transitions in cryo-slow electron velocity mapped imaging (SEVI) studies of NiO_2^-.[11]

The highly accurate cryo-SEVI measured electron binding energies (eBEs) are vital for the extraction of detailed information from the lower resolution 2D-PES measurements reported in this work. The cryo-SEVI technique[12–17] combines cryogenic cooling of anions and slow electron velocity mapped imaging (SEVI) to provide high resolution photoelectron spectra. In short, cooling eases spectral congestion, while the SEVI technique leverages the efficiency of charged particle imaging[18,19] and the higher electron kinetic energy (eKE) resolution associated with low momentum photoelectrons. By detecting only the lowest eKE electrons, very

accurate measurements of eBEs are obtained. The value of these has been demonstrated in the interpretation of photodetachment at energies significantly above channel thresholds. For example, combining cryo-SEVI data[20] to photon energy dependent changes in spectra of cyanomethide allowed for the extraction of action spectra for formally forbidden spectroscopic transitions resulting from vibrational autodetachment of an intermediate dipole bound state.[21,22] The action spectra revealed the rovibrational structure of the mediating state and evidence for vibrational mode coupling.[23]

2D-PES suffers from decreasing resolution in the eKE domain as the photon energy increases. However, SEVI is essentially blind to phenomena such as higher eKE variations in spectral intensities and photoelectron angular distributions. Thus, a combination of 2D-PES and SEVI data represents a whole that is greater than the sum of its parts. The work presented herein on NiO_2^- detachment is a case in point. Previous studies of NiO_2^- detachment have established that both the anion and neutral ground states are linear.[11,24,25] However, the recent cryo-SEVI work[11] reveals symmetry forbidden (odd quanta) transitions to bending levels of the neutral NiO_2 ground state. One explanation proposed for the source of the forbidden bending transitions is Herzberg–Teller coupling of the neutral ground state with a neutral excited state,[26] which is predicted to lie 2.24 eV above the neutral ground state by Equation-of-Motion Coupled Cluster (EOM-CCSDT) calculations with a cc-pVDZ basis set.[11] This interpretation effectively assumes that the detachment transitions are direct via a terminal neutral state without any significant subsequent electron–neutral interaction. Within this interpretation, vibronic coupling allows "intensity borrowing" for the bending transitions.

Direct detachment transitions should show characteristic behavior as the photon energy is increased above threshold. The photoelectron intensity should vary slowly, initially rising and then becoming relatively constant as the eKE increases. This cannot be verified for the forbidden transitions of NiO_2^- using SEVI. However, using the binding energies provided by cryo-SEVI, along with 2D-PES data, the hypothesis of direct detachment can be tested. As will be shown in this work, taking a combined approach suggests a different origin for the forbidden bending transitions and reveals previously hidden details of the NiO_2^- detachment process. This gives rise to an alternate hypothesis that for the right photon energies, excitation takes place to the (ro)vibrational levels of a temporary anion excited state. This state then autodetaches, producing neutral NiO_2 and allowing access to the forbidden odd quanta bending levels (among others).

This interpretation is supported in the current work by correlated electronic structure calculations. The electronic structure of molecular transitional metals presents significant challenges to modern computational chemistry. Nearly degenerate *d*-orbitals combined with ligand interactions make strong, or multireference, correlation a common phenomenon in these species. Importantly, while some ground states can be well described by a single Hartree–Fock determinant, the excited states of small molecular transition metals may exhibit varying degrees of correlation. In this work, we provide strong support for the resonance mediated detachment hypothesis in NiO_2^- through multireference complete active-space self-consistent field (CASSCF) and second-order perturbation theory (CASPT2) studies with calculated vibrational frequencies and potential energy surfaces of the relevant states.

This work represents a reinterpretation of the near threshold photoelectron spectra of the NiO_2^- anion. Following a brief description of the experimental and theoretical methods employed, we present the results of a detailed experimental study of NiO_2^- photodetachment, beyond the slow electron limit. These results show clear differences from those expected under the assumption of direct electron loss. Instead, they are more reminiscent of prior excitation to a metastable anion state. Results of the first rigorous multireference (CASSCF and CASPT2) calculations of electronically excited NiO_2^- are presented to provide likely candidates for such intermediate states and the observed behavior discussed in the context of the possible states that can be accessed.

METHODS

Experimental

This study represents a collection of individual NiO_2^- photoelectron spectra (513 over 150 different photon energies). The excitation energy ranges from 3.243 to 4.378 eV. All experiments are carried out in a differentially pumped vacuum instrument that has been discussed previously.[23] In brief, the instrument is comprised of an ion chamber, a Wiley–McLaren Time of Flight (TOF) tube,[27] and a detection region. NiO_2^-, F^- (and other) anions are generated by pulsing oxygen through a solenoid nozzle (General Valve, Series 9, 0.76 mm orifice diameter) with a backing pressure of 80 psi. Disk-shaped Teflon spacers (with a central hole) mounted to the face of the nozzle support two electrodes that produce the pulsed discharge used to generate ions. One electrode (grounded) is a steel needle, and the other is a nickel needle connected to a high voltage pulse generator (DEI PVX-4140), producing voltages between −600 and −1400 V. Anion separation is affected by TOF-MS. Photoexcitation of NiO_2^- via the output of a tunable dye laser (Sirah Cobra-Stretch, pumped by a Spectra Physics INDI-10 Nd:YAG laser) produces photoelectrons. These are focused onto a dual chevron microchannel plate detector backed with a phosphor screen (Burle Inc.) using an inline, three electrode velocity mapped imaging arrangement.[19] Electron impacts on the detector are recorded using a charge coupled device (CCD) camera (Imperx, Inc., IPX-VGA 120-L) and accumulated frame by frame. The resulting images represent 2D projections of the original 3D photoelectron distribution, which is reconstructed using pBASEX,[28] allowing for extraction of momentum domain photoelectron spectra and angular distributions. Spectra are calibrated using F^- (the result of ablation from the Teflon spacers) images recorded under the same imaging conditions.

Computational

All calculations were performed with the OpenMolcas package.[29,30] State-specific (SS) CASPT2 calculations are used to compute energies, geometries, and vibrational frequencies.[31–33] The ANO-RCC-VQZP basis set[34,35] is used with Cholesky decomposition for density fitting of integrals,[36–38] along with the second-order Douglass–Kroll–Hess scalar relativistic correction.[39,40] C_{2v} symmetry was utilized in all calculations, although we use the $D_{\infty h}$ group symbols for clarity in linear cases. The active space chosen for the anion calculations was 19 electrons in 16 orbitals, or [19,16]. This includes O 2*p* (6 orbitals), Ni 3*d* (5), Ni 4*s* (1), and a set of

Ni 4*d* (4) orbitals to account for the so-called double-*d*-shell effect, which improves the description of radial correlations in the 3*d* shell.[41–43] The $4d_{z^2}$ orbital was excluded to make the calculations more practicable; however, this orbital may be important in bond-stretching scenarios, as the orbital lies along the inter-nuclear axis. The [19,16] calculations were initialized with the solution from a smaller [19,12] active space without the second *d*-shell.

The smaller active space overestimates the energy gap between the doublet (anion) and singlet (neutral) ground states, in line with previous studies.[44] Furthermore, the smaller active space was insufficient to reliably describe the potential energy surface away from the equilibrium geometry of the state. This is also true, to a lesser extent, of the [19,16] active space. For example, stretching the Ni–O bonds in the $^1\Sigma_g$ state beyond about 1.80 Å resulted in unreliable convergence in the CASSCF, signaling a failure of the chosen active space to describe that portion of the surface. On the other hand, the [19,16] active space is sufficient to describe the low-lying excited states of the anion near the linear (equilibrium) geometry of the anion ground state and at modest bending angles.

EXPERIMENTAL RESULTS

2D-PES and eKE domain action spectra

The NiO_2^- photoelectron spectra are summarized in the 2D-PES in Fig. 1. This was constructed by converting individual momentum domain spectra to the eKE domain (via the appropriate Jacobian transformation) for each photon energy and then averaging. The averaged eKE domain spectra are normalized to unit area and linearly interpolated to a uniform grid along E_{hv} and eKE. The photon energy sampling density is indicated by the black tick marks on the right-hand axis in Fig. 1. The 2D-PES consists of a series of diagonal features for which eKE and photon energy are linearly dependent. Superimposed on these, within a narrow band (eKEs between 0 and 0.15 eV), there is a relatively high intensity vertical feature, observed for photon energies up to 3.6 eV.

The diagonal features are dominated by allowed direct photodetachment channels to the zero-point or excited symmetric stretching levels of three different electronic states of neutral NiO_2. The assignment to allowed transitions is based on analysis of the 2D-PES, which yields the eBEs for these features, and the symmetric stretching frequencies for each neutral electronic state, summarized in Table I. These eBEs are in excellent agreement with previous results.[11,24,25]

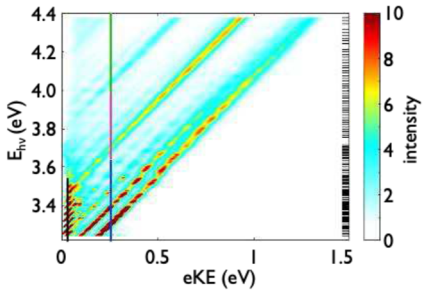

FIG. 1. 2D-PES for photodetachment from NiO_2^-. The black bars on the right-hand coordinate indicate the photon energies at which individual spectra were recorded. The vertical lines at 0.04 eV (black) and 0.26 eV (colored) represent eKEs at which the contour profiles (eKE action spectra) of Fig. 2 are illustrated.

Taking a constant eKE (vertical) cut through the 2D-PES represents an eKE action spectrum or the detachment probability for a given eKE at a particular photon energy. For example, at eKE = 0.26 eV (the colored vertical line on the 2D-PES in Fig. 1), the variation in detachment probability is represented by the color-coded spectrum in Fig. 2. The color coding highlights the different vibronic bands this action spectrum encompasses. Each band originates in the $\tilde{X}^2\Pi_g$ electronic state of the anion and terminates in

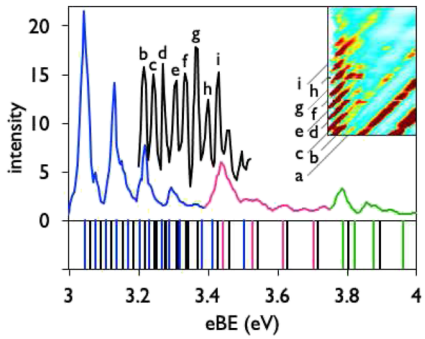

FIG. 2. Contour profiles from the 2D PES are the action spectra for an eKE of 0.04 eV (black curve) and 0.26 eV (blue, pink, and green curve). The inset in the top right corner shows the different features (labeled a–i), in the portion of the 2D PES, which includes the forbidden transitions.

TABLE I. Transition binding energies and vibrational assignments.

Band	$\tilde{X} \rightarrow \tilde{X}$					$\tilde{X} \rightarrow \tilde{a}$			$\tilde{X} \rightarrow \tilde{A}$	
Transition	0_0^0	1_0^1	1_0^2	1_0^3	1_0^4	0_0^0	1_0^1	1_0^2	0_0^0	1_0^1
eBE (eV)	3.048	3.142	3.234	3.326		3.444	3.531	3.635	3.795	3.883
$\omega_1(cm^{-1})$	758					702			710	
eBE (eV)[a]	3.046	3.139	3.232	3.321	3.412	3.445	3.530	3.616	3.788	3.876
$\omega_1(cm^{-1})$[a]	753					685			710	

[a]For comparison, values from the high resolution SEVI study are included.[11]

TABLE II. Features contributing to the low eKE region of the 2D-PES for photon energies less than 3.6 eV. Assignments are made according to Ref. 11.

	Energy (eV)	Possible contributors $(\tilde{X} \rightarrow \tilde{X})$	$(\tilde{X} \rightarrow \tilde{a})$
a	3.186	$1_0^1 2_0^3$	
b	3.222	$1_0^1 2_0^5$	
c	3.252	1_0^2, $1_0^1 2_0^7$, $1_0^2 2_0^1$	
d	3.284	$1_0^1 2_0^7$, $1_0^2 2_0^3$	
e	3.316	$2_0^1 3_0^2$, 2_0^5	
f	3.348	$1_0^3 2_0^1$, $1_0^2 2_0^7$, $1_0^3 2_0^3$	
g	3.382	$1_0^2 2_0^9$	
h	3.414	1_0^4	
i	3.447	$1_0^4 2_0^1$	0_0^0
j	3.457		2_0^1

the $\tilde{X}^1\Sigma_g$ (blue), $\tilde{a}^3\Pi_g$ (pink), or $\tilde{A}^1\Pi_g$ (green) electronic states of the neutral. In the 0.26 eV action spectrum, the main contributions to the observed structure are the symmetry allowed excitations of Table I.

An eKE action spectrum at 0.04 eV (black vertical bar in Fig. 1 and black spectrum in Fig. 2) reveals rather different behavior. There are clearly several transitions in between the allowed features, which are largely absent at higher eKE. The transitions in the 0.04 eV spectrum are predominantly associated with symmetry forbidden transitions. Possible assignments are given in Table II based on previous SEVI results.[11] These transitions mainly include symmetry forbidden combinations of symmetric stretching and odd quanta bending transitions, $1_0^{v_1} 2_0^{v_2=\text{odd}}$. The $\tilde{X}^2\Pi_g \rightarrow \tilde{X}^1\Sigma_g$ and $\tilde{X}^2\Pi_g \rightarrow \tilde{a}^3\Pi_g$ bands are represented within the 0.04 eV action spectrum, and there is some overlap toward the higher photon energy end. Nevertheless, the symmetry forbidden transitions are associated with detachment accompanied by an odd numbered change in bending quanta of the terminal neutral state. More importantly, their absence in the 0.26 eV eKE action spectrum shows that the forbidden transition probabilities dramatically decrease as the photon energy is tuned away from threshold.

Transition branching ratios

Although the diagonal features of the 2D-PES in Fig. 1 correspond to allowed transitions, the energy dependence of their intensities shows behavior not normally associated with direct detachment. Instead, several oscillations are seen as the photon energy is increased. A more quantitative representation of the variation in spectral intensities can be observed by extracting branching ratios (relative transition probabilities) as a function of photon energy.

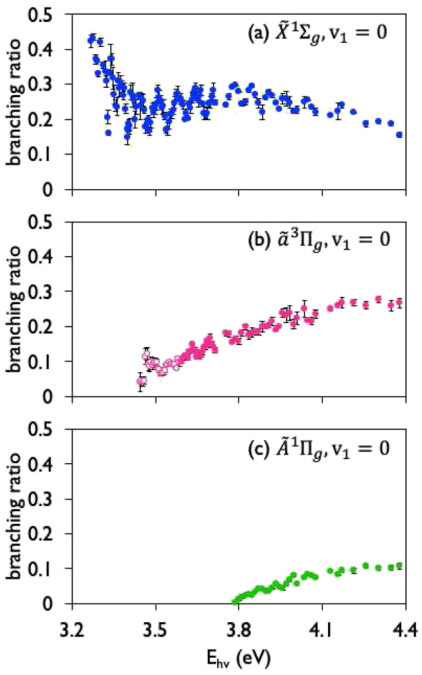

FIG. 3. Branching ratios for the 0_0^0 transitions to the (a) $\tilde{X}^1\Sigma_g$ (blue), (b) $\tilde{a}^3\Pi_g$ (pink), and (c) $\tilde{A}^1\Pi_g$ (green) states. The error bar values come from the standard deviation between measurements. Empty circles indicate photon energies for which forbidden and allowed signals overlap at low eKE.

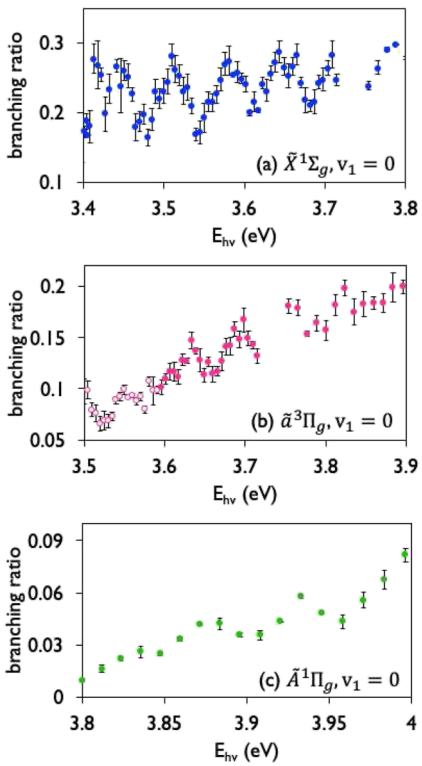

FIG. 4. Oscillatory behavior in the branching ratios for the transitions shown in Fig. 3. The narrower range of photon energies highlights the oscillations superimposed on the underlying trend.

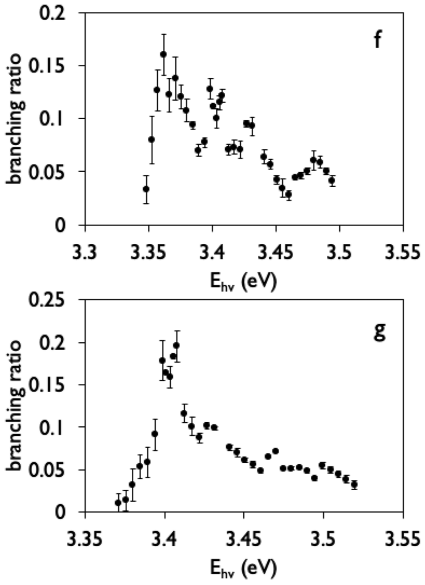

FIG. 5. Branching ratios of the Franck–Condon forbidden features f and g in the $\tilde{X}^2\Pi_g \rightarrow \tilde{X}^1\Sigma_g$ band.

Figures 3–5 show branching ratios for selected allowed and forbidden features within the 2D-PES. For a particular photon energy, these are obtained by dividing the area corresponding to an individual transition by the area under the whole spectrum. The pre-existing SEVI data provide an excellent database to overcome the limits of the spectral resolution, to some extent. The fitting procedure employed has been described in detail elsewhere.[21] In brief, the individual momentum domain spectra (at each photon energy) are fit with a sum of Gaussians. Each Gaussian represents a different detachment transition, allowed or forbidden. The Gaussian centers are based on the SEVI reported eBE,[11] with small variation allowed to obtain the best fit (tolerances of 0.0075 eV for eKE < 0.15 eV and 0.01 eV otherwise). The procedure is applied to the momentum domain spectra to take advantage of the uniform momentum domain resolution of the imaging technique. This allows a single width for all Gaussians applied to a given spectrum, reducing the overall number of fitting parameters. Branching ratios are obtained by dividing the area of a specific Gaussian by the sum of the areas of all the Gaussians. Averaging the branching ratios for a given transition obtained at a particular photon energy produces the values plotted in Figs. 3–5. The error bars represent the standard deviation within the dataset for each transition at each photon energy. At some photon energies corresponding to low eKE detachment, the fitting procedure can still be ambiguous. Open symbols in Figs. 3 and 4 indicate cases where allowed and forbidden transitions overlap at low eKE.

Allowed transitions—Underlying behavior

Figure 3 shows branching ratio action spectra for the origin transition in each of the detachment bands. There are clear similarities in the underlying behavior for the $\tilde{X} \rightarrow \tilde{a}$ and $\tilde{X} \rightarrow \tilde{A}$ bands.

TABLE III. Average peak separations in branching ratios within the $\tilde{X} \rightarrow \tilde{X}$ and $\tilde{X} \rightarrow \tilde{a}$ bands. Values are given in cm^{-1}.

$\tilde{X} \rightarrow \tilde{X}$		$\tilde{X} \rightarrow \tilde{a}$	
0_0^0	559	0_0^0	541
1_0^1	593		
1_0^2	579		
1_0^3	593		

The branching ratios initially increase as the photon energy exceeds threshold, but ultimately approach what looks like some form of limit or maximum. At first glance, the underlying behavior for the $\tilde{X} \rightarrow \tilde{X}$ origin transition looks different. There is an initial decrease in the branching ratio and then a gradual increase to a maximum. This observation needs to be interpreted carefully. First, in this case, the data do not cover the immediate threshold region for the transition. Second, for this photon energy range, the thresholds of several other transitions are crossed, spreading the spectral intensity over a broader range of energies and contributing to the initial decrease in branching ratio.

Allowed transitions—Oscillatory behavior

In the branching ratio spectra in Fig. 3, there are some relatively rapid changes superimposed on the underlying behavior. These do not conform to the expectation of gradual change associated with direct detachment. These oscillations are clear for all allowed transitions associated with the $\tilde{X} \rightarrow \tilde{X}$ band and, to a greater or lesser extent, the allowed features in the $\tilde{X} \rightarrow \tilde{a}$ and $\tilde{X} \rightarrow \tilde{A}$ bands. A clearer illustration can be found in Fig. 4 (and in the supplementary material), which expands the photon energy scale. The average spacing between oscillations in a transition is determined by performing a nonlinear least-squares fit of the branching ratio to the equation $y = a \cdot \sin(bx + c) + d \cdot \sin(fx + c)$. Fitting to the sum of the sines equation, in which the first term accounts for the underlying shape and the second for the finer detail, reveals that the periods of these oscillations are remarkably similar across all features within the $\tilde{X} \rightarrow \tilde{X}$ and $\tilde{X} \rightarrow \tilde{a}$ bands. The periods for each vibrational feature within these bands are given in Table III.

These measurements are branching ratios, so it is important to note that the oscillations persist at photon energies well in excess of those that produce the intense forbidden spectral transitions, *and* the oscillation frequency does not match the energy spacing of channel openings. Put another way, these oscillations are not simply due to the appearance of new and rapidly diminishing spectral features. Rather, they reflect the details of the detachment process.

Forbidden transitions

A common characteristic of the allowed spectral features is a gradual underlying rise in the branching ratio, albeit complicated by the introduction of new channels as the photon energy increases. For example, the origin transition for the $\tilde{X} \rightarrow \tilde{X}$ band in Fig. 3 shows an initial fall followed by a gradual rise in the branching ratio. This behavior is the result of threshold laws[45] meeting the dispersal of detachment probability across an increasing number of relatively

high probability transitions as the photon energy increases. Nevertheless, the longer range and gradual increase in the underlying branching ratios for the transitions of displayed in Fig. 3 mark these out as "allowed" transitions. In contrast, transitions associated with the 0.04 eV eKE action spectrum show rather different behavior.

Following the branching ratios associated with the low eKE features (a–i) is problematic in many cases, for reasons of spectral congestion affecting the Gaussian fitting procedure. However, features f and g, which correspond to transitions involving odd numbered changes in bending character, are sufficiently resolved from nearby allowed transitions to retain confidence in the results of the fitting procedure. These cases show a relatively rapid onset (this phenomenon is illustrated in Fig. 5) before a distinct maximum is reached at relatively low eKE. Subsequently, the branching ratio follows a decreasing trend, although again there is some oscillatory behavior superimposed on this background.

Angular distributions

Associated with each detachment transition is a photoelectron angular distribution, $I(\theta)$, where θ is the angle between the momentum vector of the electron and the polarization of the electric vector of the radiation. The angular distribution is quantitatively described using the anisotropy parameter, β, obtained by fitting $C[1+\beta P_2(\cos\theta)]$ to $I(\theta)$, in which $P_2(\cos\theta)$ is the second Legendre polynomial and C is a constant related to the overall cross section at a given photon energy. $I(\theta)$ is influenced by several factors, including the originating orbital, the eKE, and, particularly in the presence of excited anion states, exit channel interactions. The β values are plotted in Fig. 6 for the origin transitions of each vibronic band in the 2D-PES.

The plots of Fig. 6 show the evolution of β as the eKE increases above the channel threshold. The data represent (a) $\tilde{X}^2\Pi_g \rightarrow \tilde{X}^1\Sigma_g$ (blue triangles) and (b) $\tilde{X}^2\Pi_g \rightarrow \tilde{a}^3\Pi_g$ (pink triangles) and $\tilde{X}^2\Pi_g \rightarrow \tilde{A}^1\Pi_g$ (green triangles). Similar to the branching ratios, each datum represents averaging over individual β values taken from several images recorded at the same photon energy, and the error bars represent standard deviations from the mean. Each image provides four separate measurements of β (for each transition in a spectrum), and each datum in Fig. 6 is comprised of an average of at least eight individual β value measurements for the same transition. Similar plots for other transitions are included in the supplementary material.

The anisotropy parameters associated with detachment via each $\tilde{X}^1\Sigma_g$ symmetric stretching level are remarkably similar, being almost isotropic across the whole excitation energy range. There is, however, a clear difference in the trends observed for this band [Fig. 6(a)] and the $\tilde{X}^2\Pi_g \rightarrow \tilde{a}^3\Pi_g$ and $\tilde{X}^2\Pi_g \rightarrow \tilde{A}^1\Pi_g$ bands [Fig. 6(b)]. The production of NiO_2 in either of these excited states shows polarization of the angular distribution (parallel to the electric vector of the radiation) as the eKE (and therefore photon energy) increases above threshold. This behavior is more pronounced for detachment via the zero-point level of the triplet compared with the singlet. Detachment to the first excited symmetric stretching level of the triplet state shows a similar preference for polarization along the photon electric vector (see the supplementary material), but the effect is much less pronounced than for detachment to the zero-point level.

The long-range behavior in the β values for the $\tilde{X} \rightarrow \tilde{a}$ and $\tilde{X} \rightarrow \tilde{A}$ transitions is strongly reminiscent of the behavior seen in detachment from σ orbitals in AgF^-,[46,47] CuF^-,[47] and CN^-.[48] Of particular note, however, in Fig. 6(b), there are significant oscillations in the value of β in the $\tilde{X} \rightarrow \tilde{a}$ data superimposed on the more gradual, longer range trends. Again, by analogy with AgF^-[46] detachment, these are indicative of the influence of an excited state mediating the detachment process. Figure 7 compares the photon energy dependence of the oscillations in the branching ratio and β for the $\tilde{X} \rightarrow \tilde{a}, 0_0^0$ channel. The peak-to-peak separation is remarkably similar and provides strong support for the notion that

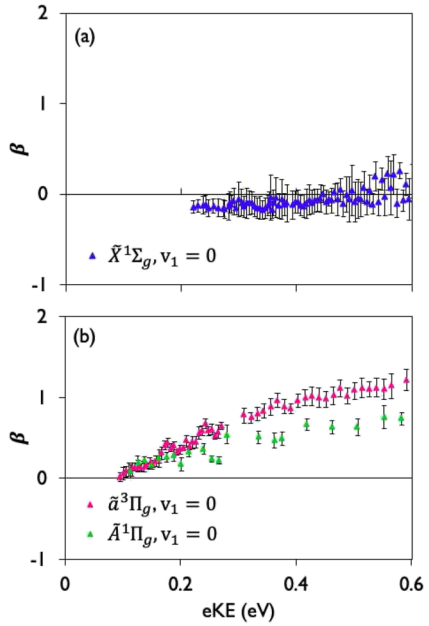

FIG. 6. Experimental β values for detachment to each for transitions to the zero point level of the (a) $\tilde{X}^1\Sigma_g$ (blue) and (b) and (c) $\tilde{a}^3\Pi_g$ (pink) and $\tilde{A}^1\Pi_g$ (green) states of NiO_2 from the zero point level of the $\tilde{X}^2\Pi_g$ state of NiO_2^-.

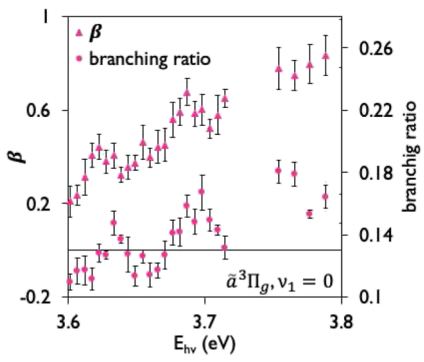

FIG. 7. Comparison of the oscillation in β values (pink triangles) and branching ratios (pink circles) for the $\tilde{X} \rightarrow \tilde{a}0_0^0$ transition.

the oscillations are not merely the result of a redistribution of the spectral density as new channels open.

The nature of the detachment process

The majority of previously reported computational studies of NiO_2 predict the ground state to be linear.[11,44,49–53] Similarly, recent calculations established the excited neutral $\tilde{a}$ and $\tilde{A}$ states as linear.[11,44,53] There have been fewer anion ground state calculations, but these generally also agree on a linear geometry.[11,51] The 0.26 eV eKE action spectrum in Fig. 2 shows detachment transitions to symmetric stretching levels of neutral NiO_2 in the $\tilde{X}, \tilde{a}$, and $\tilde{A}$ electronic states. These observations are in perfect agreement with earlier reported photoelectron spectra away from the band thresholds[11,24,25] and also in line with triatomic linear to linear transitions in which the Ni–O bond length changes.

On the other hand, the appearance of the closely spaced features in the 0.04 eV eKE action spectrum, which are consistent with recent SEVI results,[11] shows that Franck–Condon forbidden, odd quanta bending transitions are possible near the $\tilde{X}$ and $\tilde{a}$ thresholds. The presence of these bending features suggests that the detachment process is not as simple as excitation to zero-order, linear neutral states. Instead, there must be a source of bending character—mixing with a state/states with a local or global potential energy minimum at a non-linear geometry, vibronic coupling between appropriate states, or a non-adiabatic process changing the selection rules for the detachment. For example, Herzberg–Teller coupling with a Π_u neutral state, identified in 2.24 eV above the neutral $\tilde{X}$ state, has been invoked as the origin of the bending character.[11] Within this scenario, the terminal neutral $\tilde{X}$ and $\tilde{a}$ states achieve some degree of bending character through coupling with the Π_u state. This effectively treats the observed spectra as the result of direct detachment to the neutral states resulting from this mixing.

This explanation is consistent with the SEVI results. However, the transitions should, therefore, show the characteristics of direct detachment. In a SEVI experiment, high resolution is achieved by limiting detection to very low eKE electrons. Data are therefore only recorded over a very small range of photon energies for a given transition. While subject to lower resolution, the 2D-PES approach allows for observations of branching ratios and anisotropy parameters over a wider range of excitation energies. Over this range, the expectations for direct detachment are that branching ratios and β parameters should evolve gradually and certainly not display oscillatory behavior.

The observed behaviors in the branching ratios of the $\tilde{X} \rightarrow \tilde{a}$ and $\tilde{X} \rightarrow \tilde{X}$ channels and β values for the $\tilde{X} \rightarrow \tilde{a}$ channel are strongly reminiscent of systems[1,21,46,47,54–56] in which temporary, excited anion states can mediate the detachment process. Thus, it is reasonable to propose a competition between detachment directly to the continuum,

$$NiO_2^-\left(\tilde{X}^2\Pi_g, v'' = 0\right) + h\nu \xrightarrow{detachment} NiO_2 + e^-,$$

and an indirect process,

$$NiO_2^-\left(\tilde{X}^2\Pi_g, v'' = 0\right) + h\nu \xrightarrow{absorption} NiO_2^{-*} \xrightarrow{detachment} NiO_2 + e^-,$$

in which there is initial excitation to an excited anion state (NiO_2^{-*}) with sufficient energy to subsequently undergo electron loss via autodetachment to some terminal neutral state. The two pathways may access the same neutral state, but the selection rules and angular momentum exchanges are likely to be different, resulting in different energy dependences for transition probabilities and angular distributions.

The absence of observable oscillatory behavior in β for the $\tilde{X} \rightarrow \tilde{X}$ band data might seem to argue against this interpretation. However, in cases where the underlying distribution is isotropic, the effect of electronic resonances on the angular distribution can often be small (the effect is often to enhance the isotropic s-wave component of the continuum wave function). Furthermore, for isotropic distributions, the uncertainties associated with the extracted anisotropy parameters tend to be larger, making small changes hard to pick out. This may go some way to explaining the lack of obvious oscillatory behavior in the anisotropy parameters in Fig. 6(a) for the $\tilde{X} \rightarrow \tilde{X}$ channel.

COMPUTATIONAL RESULTS

Electronic states

For the indirect process to be possible, suitable intermediate excited anion states must be available. This is explored via multi-reference CASPT2 calculations. While treatments of the anion ground and neutral ground/excited electronic states have been reported previously,[11,44,49–53,57–59] the calculations performed in the current work represent the first systematic treatment of excited anion states in the vicinity of the neutral ground state for NiO_2.

Our CASPT2 calculations characterize the symmetric stretching and bending potential energy surfaces of three states relevant

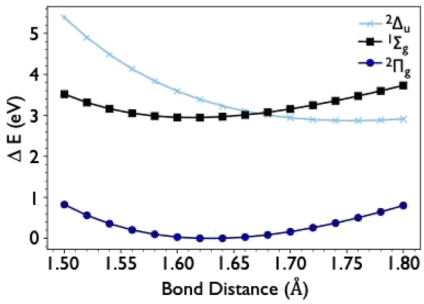

FIG. 8. Stretching potential curves (at linear geometry) of the anion ground ($^2\Pi_g$, purple circles), anion excited ($^2\Delta_u$, blue crosses), and neutral ground ($^1\Sigma_g$, black squares) states.

TABLE IV. Equilibrium bond lengths and symmetric stretching (υ_1) and bending (υ_2) vibrational frequencies for the NiO_2 and NiO_2^- ground states and NiO_2^- $^2\Delta_u$ excited state.

Electronic state	r_e (Å)	Angle (°)	$\upsilon_1\left(cm^{-1}\right)$	$\upsilon_2\left(cm^{-1}\right)$
$^1\Sigma_g$	1.608	180	787	58
$^2\Pi_g$	1.629	180	798	44
$^2\Delta_u$	1.752	180	605	187

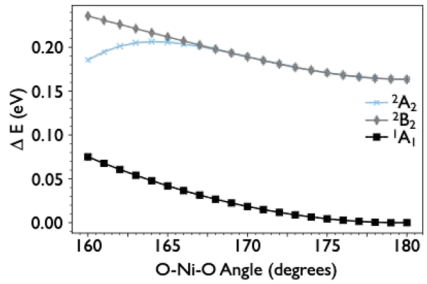

FIG. 9. Stretching potential curves of the neutral ground ($^1\Sigma_g$, black squares) state and the two degenerate states (blue crosses and gray diamonds) that arise from Renner–Teller splitting of the anion excited state, $^2\Delta_u$.

to the $NiO_2 + e^-$ system. In particular, Fig. 8 shows the variation along the symmetric stretching coordinate at a fixed, linear bond angle for the anion ground state ($^2\Pi_g$, purple circles), the neutral ground state ($^1\Sigma_g$, black squares), and most importantly an excited anion state ($^2\Delta_u$, blue crosses). The equilibrium bond lengths (r_{eq}) for these states are reported in Table IV. The $^1\Sigma_g$ state equilibrium bond length of 1.608 Å is in excellent agreement with previous multireference configuration interaction (MRCI),[44] generalized and complete active space,[53] and EOM-CCSD(T)[11] calculations. For the $^2\Pi_g$ state, the equilibrium bond length is slightly shorter than the CCSD(T) result, 1.643 Å compared to 1.639 Å,[11] while the $^2\Delta_u$ state has a linear minimum at 1.752 Å.

The CASPT2 calculations suggest that the adiabatic electron affinity of NiO_2 (the eBE for the $\tilde{X} \rightarrow \tilde{X}, 0_0^0$ transition) is 3.06 eV, showing the ground state calculations to be in excellent agreement with the experiment (Table I). For the excited anion states, at the geometry of the anion ground state, the $^2\Delta_u$ state is 3.15 eV higher in energy (vertically) and 0.16 eV above the neutral ground state. Finally, we note that electronic excitation to a $^2\Delta_u$ state from the $^2\Pi_g$ ground state is electric-dipole allowed.

The nature of the $^2\Delta_u$ state has been explored more fully by examining the potential energy surface along the bending coordinate. Upon bending a doubly degenerate triatomic electronic state is expected to split into two components, a phenomenon known as the Renner–Teller effect.[26,60] Figure 9 shows the variation in the potential energy of the states $^2A_2$ (blue crosses) and $^2B_2$ (grey diamonds) along the bending coordinate. Typical of a Δ state,[26,61] the splitting is quite small at small angles, and the separation of the states becomes more pronounced for ∠ONiO < 165°. The $^2B_2$ state energy continues to rise as the bond angle decreases; however, the $^2A_2$ state energy begins to decrease and, although not illustrated in Fig. 9, reaches a second minimum at a bond angle of 154°.

DISCUSSION

The most striking features in the data in Figs. 3 and 4 are the oscillations in the branching ratios. These are superimposed on an underlying direct detachment background. The presence of excited anion states offers a possible explanation. Electronic excitation to $^2\Delta_u\left(^2A_2/^2B_2\right)$ is formally allowed from the anion ground state. However, the probability of excitation will depend on the photon energy coming into resonance with vibrational levels of the excited state and within the limits of vertical excitation, favorable Franck–Condon factors. Subsequent autodetachment provides a pathway for electron loss.

Broadly speaking, two autodetachment mechanisms can be considered: electronic autodetachment, in which the anion electronic state lies above the neutral ground state. In this scenario, electron loss is rapid compared to the timescale of nuclear motion. The vibrational levels accessed in the neutral will be governed by the overlap of the vibrational wave functions of the excited anion and neutral ground states. In such a situation, it would not be unexpected, permitting sufficient available energy, to observe a range of different terminal neutral states resulting from the excitation of a particular anion vibronic state. In the context of the data of Fig. 4, this would lead to different excited anion states contributing to detachment via a particular terminal neutral state. On the other hand, when the zero-point level of the excited anion lies below the neutral ground state zero-point level, electron loss requires transfer of vibrational energy to the excess electron. This process tends to occur on the timescale of a molecular vibration and is termed vibrational autodetachment. Usually, vibrational autodetachment follows propensity rules[62] in which the electron loss is accompanied by reduction of the vibrational energy by a single quantum within a single mode. Somewhat contrarily, the results presented in this paper seem to reflect behaviors associated with both processes.

The oscillations observed in the cross sections of the symmetry allowed detachment pathways are consistent with excited state vibrational levels autodetaching via an envelope of neutral ground state symmetric stretching, or the zero point, levels. The contribution of the indirect pathway varies with excitation energy, the result of the requirement for resonance with the internal levels of the excited anion state. Put another way, agreement between the calculated excited state symmetric stretching frequencies and the spacing of the maxima in Fig. 4 is supportive of this interpretation. Scanning the photon energy in this region is tantamount to spectroscopically probing the vibrational levels of the short-lived excited state.

In the case of the bending transitions, however, a Franck–Condon based interpretation is not consistent with the data. Assuming that the excitation transition occurs from the zero-point level of a linear state to a linear excited state, symmetry suggests that only bending levels with even quanta can be excited. Similarly, for electronic autodetachment from these states, only even quanta bending levels of the neutral are accessible. This is clearly counter to both our results and the earlier SEVI work. In our instrument, there is no temperature control, and it is possible that odd bending levels of the anion ground state are populated. However, the current results are in excellent agreement with the cryo-SEVI measurements, which can safely be assumed to take place from the anion ground state zero-point level. In addition, the appearance, and subsequent rapid loss, of the odd quanta bending channels is more consistent with a vibrational autodetachment. Interestingly, the $^2A_2$ component of the Renner–Teller pair that constitutes the excited anion state has (on the range 0-π) two minima, separated by a low barrier. The bending wave functions associated with this potential are likely to provide significant amplitude at significantly non-linear geometries.

Further work is needed to fully understand the detachment dynamics in near threshold detachment from NiO_2^-. Whether the

excited anion global minimum lies above or below the neutral zero-point level is an open question. In the calculations presented here, the $^2A_2$ minimum is about 0.04 eV higher in energy than the calculated linear minimum for the $^2\Delta_2$ state. In turn, this is 0.16 eV above the neutral ground state at the neutral anion r_e. However, at the excited anion r_e, the neutral ground state is higher in energy. Previous work has estimated the accuracy of the CASPT2-based model for excited state energies of small molecules to be about 0.01 eV.[63] More recently, for excited states of larger molecules, the CASPT2 error has been estimated to be about 0.1 eV.[64] Given these ranges of errors, the true ordering of the electronic states and the relative energies of the minima on the $^2A_2$ surface are still open to question. Nevertheless, it is clear that the intermediate and terminal states in the detachment process all lie in close proximity and open up the possibility of the competing autodetachment pathways. Most importantly, the experimental and computational results presented here clearly indicate the presence of low-lying anion states mediating the detachment process.

CONCLUSIONS

A more descriptive picture of detachment from NiO_2^- has been captured by combining 2D-PES results with those from SEVI and CASPT2 calculations. On its own, 2D-PES provides evidence of resonance mediated detachment with oscillations in transition branching ratios and β. The repeating oscillations in branching ratios of allowed transitions indicate excitation to a single vibrational level of a resonance, which subsequently relaxes via electron loss to multiple vibrational levels of the neutral, consistent with electronic autodetachment. The possibility of excited anion states mediating the detachment process represents an alternate detachment pathway to that previously presented to explain SEVI results of the same system.[11] In fact, evidence for the presence of temporary anion states is provided through a comparison of the 2D-PES with SEVI results. This confirms the assignment of Franck–Condon forbidden transitions to the low eKE transitions in the 2D-PES. However, because the forbidden transitions are only present at low eKE, it is likely that some form of vibrational autodetachment is taking place. While Herzberg–Teller coupling to an excited neutral state could explain the presence of the forbidden transitions, this alone does not account for the observed branching ratio and β trends.

Candidates for the excited anion states have been calculated using CASPT2. These are found to be energetically close to the relevant neutral states. Specifically, bending of a linear $^2\Delta_u$ excited anion state results in Renner–Teller splitting into $^2A_2$ and $^2B_2$ states. The $^2B_2$ state has an additional minimum at a bent conformation. Thus, the CASPT2 calculations provide evidence for a candidate nonlinear excited anion state that can contribute the necessary bending character to access the forbidden transitions. In addition, the symmetric stretching frequency of the excited states is calculated to be 605 cm^{-1}, consistent with the observed oscillations in the branching ratio. This suggests that within the photon energy range employed, different optically allowed levels of the excited states are accessed. Furthermore, it appears that a combination of electronic and vibrational autodetachment processes may occur within this excitation range.

In summary, the combined 2D-PES and multireference CASPT2 studies presented here provide strong evidence for the existence of low lying excited anion states of the $NiO_2 + e^-$ system. These states mediate the detachment process, giving rise to distinct, non-direct detachment behavior in the branching rations, and the appearance of forbidden bending features. In fact, the results presented here represent a spectroscopic probe of these transient electronic states.

SUPPLEMENTARY MATERIAL

The supplementary material provided gives a comprehensive overview of the experimental data extracted from the 2D-PES of NiO_2^- represented in Figs. 1 and 2 of this article. The data include channel branching ratios for allowed and forbidden spectroscopic transitions, and measurements of the anisotropy parameter (β) are a function of photon energy for allowed transitions.

ACKNOWLEDGMENTS

The authors acknowledge the support from the National Science Foundation, CSDM-A Program, Division of Chemistry (RM under Grant No. CHE-1566157).

AUTHOR DECLARATIONS

Conflict of Interest

The authors have no conflicts to disclose.

Author Contributions

C. Annie Hart: Data curation (equal); Formal analysis (equal); Investigation (equal); Methodology (equal); Writing – original draft (equal); Writing – review & editing (equal). **Anthony W. Schlimgen**: Data curation (equal); Formal analysis (equal); Methodology (equal); Writing – original draft (equal); Writing – review & editing (equal). **Diep Bich Dao**: Investigation (equal). **Kade Head-Marsden**: Project administration (equal); Resources (equal); Writing – review & editing (equal). **Richard Mabbs**: Conceptualization (lead); Project administration (equal); Resources (equal); Writing – original draft (equal); Writing – review & editing (equal).

DATA AVAILABILITY

The data that support the findings of this study are available within the article and its supplementary material.

REFERENCES

[1] J. Lyle, T. C. Jagau, and R. Mabbs, Faraday Discuss. **217**, 533 (2019).
[2] C. S. Anstoter, G. Mensa-Bonsu, P. Nag, M. Rankovic, T. P. Ragesh Kumar, A. N. Boichenko, A. V. Bochenkova, J. Fedor, and J. R. R. Verlet, Phys. Rev. Lett. **124**, 203401 (2020).
[3] M. A. Dobulis, M. C. Thompson, T. Sommerfeld, and C. C. Jarrold, J. Chem. Phys. **152**, 204309 (2020).

[4]M. A. Dobulis, C. J. McGee, T. Sommerfeld, and C. C. Jarrold, J. Phys. Chem. A **125**, 9128 (2021).
[5]J. Simons, J. Phys. Chem. A **127**, 3940 (2023).
[6]A. Lietard, G. Mensa-Bonsu, and J. R. R. Verlet, Nat. Chem. **13**, 737 (2021).
[7]G. Mensa-Bonsu, M. R. Wilson, D. J. Tozer, and J. R. R. Verlet, J. Chem. Phys. **151**, 204302 (2019).
[8]J. P. Rogers, C. S. Anstoter, J. N. Bull, F. E. Curchod, and J. R. R. Verlet, J. Phys. Chem. A **123**, 1602 (2019).
[9]J. P. Rogers, C. S. Anstoter, and J. R. R. Verlet, J. Phys. Chem. Lett. **9**, 2504 (2018).
[10]C. W. West, J. N. Bull, E. Antonkov, and J. R. R. Verlet, J. Phys. Chem. A **118**, 11346 (2014).
[11]M. C. Babin, M. DeWitt, J. A. Lau, M. L. Weichman, J. B. Kim, L. Cheng, and D. M. Neumark, Phys. Chem. Chem. Phys. **24**, 17496 (2022).
[12]A. Osterwalder, M. J. Nee, J. Zhou, and D. M. Neumark, J. Chem. Phys. **121**, 6317 (2004).
[13]D. M. Neumark, J. Phys. Chem. A **112**, 13287 (2008).
[14]D.-L. Huang, G.-Z. Zhu, Y. Liu, and L.-S. Wang, J. Mol. Spectrosc. **332**, 86 (2017).
[15]Y.-R. Zhang, D.-F. Yuan, and L.-S. Wang, Phys. Chem. Chem. Phys. **24**, 6505 (2022).
[16]G.-Z. Zhu, Y. Liu, and L. S. Wang, Phys. Rev. Lett. **119**, 023002 (2017).
[17]M. L. Weichman and D. M. Neumark, Annu. Rev. Phys. Chem. **69**, 101 (2018).
[18]D. W. Chandler and J. I. Cline, in *Modern Trends in Chemical Reaction Dynamics: Part 1–Experiment and Theory*, Adv. Ser. Phys. Chem. **14**, edited by X. Yang and K. Liu (World Scientific, 2004), p. 61.
[19]A. T. J. B. Eppink and D. H. Parker, Rev. Sci. Instrum. **68**, 3477 (1997).
[20]J. B. Kim, M. L. Weichman, and D. M. Neumark, J. Chem. Phys. **140**, 104305 (2014).
[21]J. Lyle, O. Wedig, S. Gulania, A. I. Krylov, and R. Mabbs, J. Chem. Phys. **147**, 234309 (2017).
[22]K. R. Lykke, D. M. Neumark, T. Andersen, V. J. Trapa, and W. C. Lineberger, J. Chem. Phys. **87**, 6842 (1987).
[23]J. Lyle, S. R. Chandramoulee, C. A. Hart, and R. Mabbs, J. Vis. Exp. **137**, e57989 (2018).
[24]H. Wu and L.-S. Wang, J. Chem. Phys. **107**, 16 (1997).
[25]T. M. Ramond, G. E. Davico, F. Hellberg, F. Svedberg, P. Salen, P. Soderqvist, and W. C. Lineberger, J. Mol. Spectrosc. **216**, 1 (2002).
[26]G. Herzberg, *Electronic Spectra of Polyatomic Molecules* (D. Van Nostrand Company Inc., Princeton, NJ, 1966).
[27]W. C. Wiley and I. H. McLaren, Rev. Sci. Instrum. **26**, 1150 (1955).
[28]G. A. Garcia, L. Nahon, and I. Powis, Rev. Sci. Instrum. **75**, 4989 (2004).
[29]I. Fdez Galván, M. Vacher, A. Alavi, C. Angeli, F. Aquilante, J. Autschbach, J. J. Bao, S. I. Bokarev, N. A. Bogdanov, R. K. Carlson, L. F. Chibotaru, J. Creutzberg, N. Dattani, M. G. Delcey, S. S. Dong, A. Dreuw, L. Freitag, L. M. Frutos, L. Gagliardi, F. Gendron, A. Giussani, L. González, G. Grell, M. Guo, C. E. Hoyer, M. Johansson, S. Keller, S. Knecht, G. Kovacevic, E. Källman, G. Li Manni, M. Lundberg, Y. Ma, S. Mai, J. P. Malhado, P. Å. Malmqvist, P. Marquetand, S. A. Mewes, J. Norell, M. Olivucci, M. Oppel, Q. M. Phung, K. Pierloot, F. Plasser, M. Reiher, A. M. Sand, I. Schapiro, P. Sharma, C. Stein, L. K. Sørensen, D. G. Truhlar, M. Ugandi, L. Ungur, A. Valentini, S. Vancoillie, V. Veryazov, O. Weser, T. A. Wesołowski, P. O. Widmark *et al.*, J. Chem. Theory Comput. **15**, 5925 (2019).
[30]F. Aquilante, J. Autschbach, A. Baiardi, S. Battaglia, V. A. Borin, L. F. Chibotaru, I. Conti, L. De Vico, M. Delcey, I. Fdez Galván, N. Ferré, L. Freitag, M. Garavelli, X. Gong, S. Knecht, E. D. Larsson, R. Lindh, M. Lundberg, P. Å. Malmqvist, A. Nenov, J. Norell, M. Odelius, M. Olivucci, T. B. Pedersen, L. Pedraza-González, Q. M. Phung, K. Pierloot, M. Reiher, I. Schapiro, J. Segarra-Martí, F. Segatta, L. Seijo, S. Sen, D.-C. Sergentu, C. J. Stein, L. Ungur, M. Vacher, A. Valentini, and V. Veryazov, J. Chem. Phys. **152**, 214117 (2020).
[31]P. A. Malmqvist, K. Pierloot, A. R. M. Shahi, C. J. Cramer, and L. Gagliardi, J. Chem. Phys. **128**, 204109 (2008).
[32]B. O. Roos, in *Advances in Chemical Physics: Ab Initio Methods in Quantum Chemistry-II*, edited by K. P. Lawley (Wiley, Chichester, England, 1987).
[33]B. O. Roos, P. R. Taylor, and P. E. Sigbahn, Chem. Phys. **48**, 157 (1980).
[34]P.-O. Widmark, B. J. Persson, and B. O. Roos, Theor. Chim. Acta **79**, 419 (1991).
[35]R. Pou-Amerigo, M. Merchan, I. Nebot-Gil, P.-O. Widmark, and B. O. Roos, Theor. Chim. Acta **92**, 149 (1995).
[36]F. Aquilante, T. B. Pedersen, R. Lindh, B. O. Roos, A. Sanchez de Meras, and H. Koch, J. Chem. Phys. **129**, 024113 (2008).
[37]F. Aquilante, R. Lindh, and T. B. Pedersen, J. Chem. Phys. **129**, 034106 (2008).
[38]F. Aquilante, T. B. Pedersen, and R. Lindh, J. Chem. Phys. **126**, 194106 (2007).
[39]M. Douglas and N. M. Kroll, Ann. Phys. **82**, 89 (1974).
[40]B. A. Hess, Phys. Rev. A **33**, 3742 (1986).
[41]K. Pierloot, "Nondynamic correlation effects in transition metal coordination compounds," in *Computational Organometallic Chemistry*, edited by T. R. Cundari (Taylor & Francis, Boca Raton, 2001), p. 123.
[42]T. H. Dunning, Jr., B. H. Botch, and J. F. Harrison, J. Chem. Phys. **72**, 3419 (1980).
[43]B. H. Botch, T. H. Dunning, Jr., and J. F. Harrison, J. Chem. Phys. **75**, 3466 (1981).
[44]O. Hübner and H. J. Himmel, J. Phys. Chem. A **116**, 9181 (2012).
[45]E. P. Wigner, Phys. Rev. **73**, 1002 (1948).
[46]D. B. Dao and R. Mabbs, J. Chem. Phys. **141**, 154304 (2014).
[47]T. C. Jagau, D. B. Dao, N. Holtgrewe, A. I. Krylov, and R. Mabbs, J. Phys. Chem. Lett. **6**, 2786 (2015).
[48]C. A. Hart, J. Lyle, J. Spellberg, A. I. Krylov, and R. Mabbs, J. Phys. Chem. Lett. **12**, 10086 (2021).
[49]A. Citra, G. V. Chertihin, L. Andrews, and M. Neurock, J. Phys. Chem. A **101**, 3109 (1997).
[50]F. Allouti, L. Manceron, and M. E. Alikhani, Phys. Chem. Chem. Phys. **8**, 448 (2006).
[51]K. Deng, J. Yang, and Q. Zhu, J. Chem. Phys. **118**, 6868 (2003).
[52]G. L. Gutsev, B. K. Rao, and P. Jena, J. Phys. Chem. A **104**, 11961 (2000).
[53]K. D. Vogiatzis, G. Li Manni, S. J. Stoneburner, D. Ma, and L. Gagliardi, J. Chem. Theory Comput. **11**, 3010 (2015).
[54]J. Lyle, S. R. Chandramoulee, J. R. Hamilton, B. A. Traylor, T. L. Guasco, T. C. Jagau, and R. Mabbs, J. Chem. Phys. **149**, 084302 (2018).
[55]F. Mbaiwa, J. Wei, M. Van Duzor, and R. Mabbs, J. Chem. Phys. **132**, 134304 (2010).
[56]F. Mbaiwa, D. Dao, N. Holtgrewe, J. Lasinski, and R. Mabbs, J. Chem. Phys. **136**, 114303 (2012).
[57]E. L. Uzunova, H. Mikosch, and G. S. Nikolov, J. Chem. Phys. **128**, 094307 (2008).
[58]C. W. Bauschlicher, Jr., S. R. Langhoff, H. Partridge, and M. Sodupe, J. Phys. Chem. **97**, 856 (1993).
[59]M. R. A. Blomberg, P. E. M. Siegbahn, and A. Strich, Chem. Phys. **97**, 287 (1985).
[60]R. Renner, Z. Phys. **92**, 172 (1934).
[61]J. A. Pople and H. C. Longuet-Higgins, Mol. Phys. **1**, 372 (1958).
[62]J. Simons, J. Am. Chem. Soc. **103**, 3971 (1981).
[63]K. Andersson, P. A. Malmqvist, and B. O. Roos, J. Chem. Phys. **96**, 1218 (1992).
[64]R. Sarkar, P.-F. Loos, M. Boggio-Pasqua, and D. Jacquemin, J. Chem. Theory Comput. **18**, 2418 (2022).